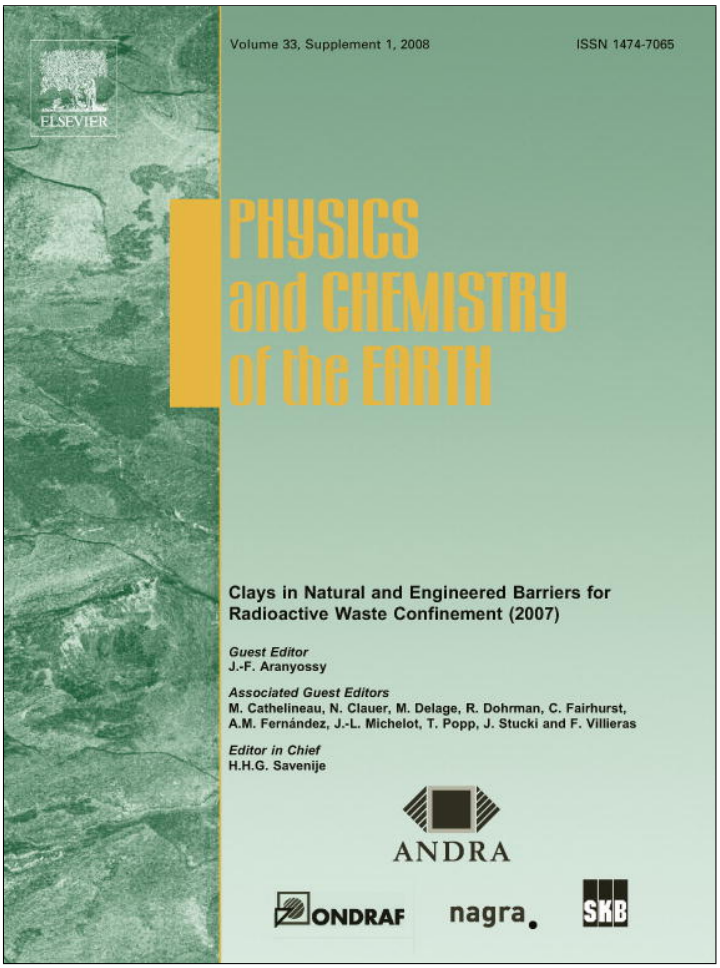
Provided for non-commercial research and education use.
Not for reproduction, distribution or commercial use.



This article appeared in a journal published by Elsevier. The attached copy is furnished to the author for internal non-commercial research and education use, including for instruction at the authors institution and sharing with colleagues.

Other uses, including reproduction and distribution, or selling or licensing copies, or posting to personal, institutional or third party websites are prohibited.

In most cases authors are permitted to post their version of the article (e.g. in Word or Tex form) to their personal website or institutional repository. Authors requiring further information regarding Elsevier's archiving and manuscript policies are encouraged to visit:

http://www.elsevier.com/copyright

Author's personal copy

Physics and Chemistry of the Earth 33 (2008) S45–S53

Contents lists available at ScienceDirect

Physics and Chemistry of the Earth

journal homepage: www.elsevier.com/locate/pce

Laboratory pressure pulse decay permeability measurement of Boda Claystone, Mecsek Mts., SW Hungary

F. Fedor [a,*], G. Hámos [a], A. Jobbik [b], Z. Máthé [a], G. Somodi [a], I. Szűcs [a]

[a] MECSEKÉRC Ltd., 19. Esztergár L.u., H-7633, Pécs, Hungary
[b] University of Miskolc, Research Institute of Applied Chemistry, H-3515, Miskolc, Hungary

ARTICLE INFO

Article history:
Available online 12 October 2008

Keywords:
BCF
Pressure pulse decay
Permeability
Porosity

ABSTRACT

The Boda Claystone Formation (BCF), explored as a possible geological disposal of HLW in Hungary, has peculiar physical and chemical characteristics. Due to the petrophysical behaviour many new methods and experimental development were applied, while the traditional methods, e.g. steady state flow test on the basis of Darcy's law, are too time-consuming. The pressure pulse decay (PPD) technique destinated to estimating gas and water permeability is one of these new methods developed for the BCF study. The main advantage of the PPD permeability compared with traditional permeability measurements is that very fast (in case of $k_g \sim 10^{-19}$ m^2 15–25 min, $k_w \sim 10^{-21}$ m^2 6–7 h), only 0.1–0.5 MPa pressure difference applied in the two sides of the examined core, quasi in situ circumstances can be provided and their uncertainty estimated.

For the correct interpretation of results of the three cores originated from different underground boreholes of the formerly URL's Alpha-1 drift, geochemical, minerological and petrophysical analysis were carried out.

The time-consumption of drying, the fact that the dry core absorbed humidity of the atmosphere very fast, as well as the unsuccess of saturation under vacuum drew attention to the importance of the necessity of careful preparation and handling as well as the necessity of geochemical and mineralogical analysis.

© 2008 Elsevier Ltd. All rights reserved.

1. Introduction

Research aimed at the geological disposal of HLW produced in the Paks Nuclear Power Plant (Paks NPP) has focused on the Upper Permian Boda Claystone Formation (BCF) since 1993. The horizontal and vertical dimensions of the BCF, one of the main part of the 4000–5000 m thick Permian (260–250 Myr) sedimentary sequence of the West Mecsek Mts. consists consolidated terrestrial – fluvial – lagoonal pelitic and chemical sediments. These sediments are approx. 150 km^2 and 700–900 m thick, respectively. The BCF is characterized by diagenetical altered monotonous cycles of relatively homogeneous sediments could be accumulated in a long time shallow-water lacustrine environment under semi-arid to arid climatic conditions (alkaline reactions, oxidation) during the Upper Permian (250–260 Myr), so-called playa basin, within a continental, undrained, half-graben sedimentary basin. Mineralogical composition of BCF is quite uniform of the BCF according to the previous studies (Máthé, 1998; Árkai et al., 2000; Varga et al., 2005, 2006). The albitic claystone composed by illite and/or muscovite (30–40%), chlorite (5–10%), authigenic albite (25–40%), quartz (5–10%), carbonates (5–15%, generally calcite or dolomite), hematite (5–10%) and inconsiderable amounts of smectite, kaolinite, vermiculite, plagioclase, ilmenite, apatite, zirkon, biotite and orthoclase. The most characteristic mineral of the formation is the fully authigenous albite (Árkai et al., 2000), which could be recognized as a white or paly pink, μm–mm size, irregular shape, disperse lens or dots (albitic nests) or as an albitic cement.

Lithologically, especially reddish brown albitic claystone alternating with albitolite, rarely thin layers of siltstone, sandstone and dolomite could be distinguished. Late diagenetical alteration of the formation was established according to the illite and chlorite alteration indexes as well as vitrinite reflection (R_o) measured on dispersed organic matter (DOM) of the thin reductive interlayer (Árkai et al., 2000; Varga et al., 2006).

The bedrock and the caprock are jointed to the water saturated sandstones reach up to 1000 m thick. Tectonically, the explored uplifted sediments locate in the core of the WE axis West Mecsek Anticline and bordered by the Magyarszék–Hetvehely and Mecsekalja Faults as shown in Fig. 1 and Fig. 2 (Kovács, 1999).

* Corresponding author. Fax: +36 72 535300.
E-mail addresses: fedorferenc@mecsekerc.hu (F. Fedor), hamosgabor@mecsekerc.hu (G. Hámos), jobbik@akki.hu (A. Jobbik), mathezoltan@mecsekerc.hu (Z. Máthé), somodigabor@mecsekerc.hu (G. Somodi), szucsistvan@mecsekerc.hu (I. Szűcs).

1474-7065/$ - see front matter © 2008 Elsevier Ltd. All rights reserved.
doi:10.1016/j.pce.2008.10.059

Author's personal copy

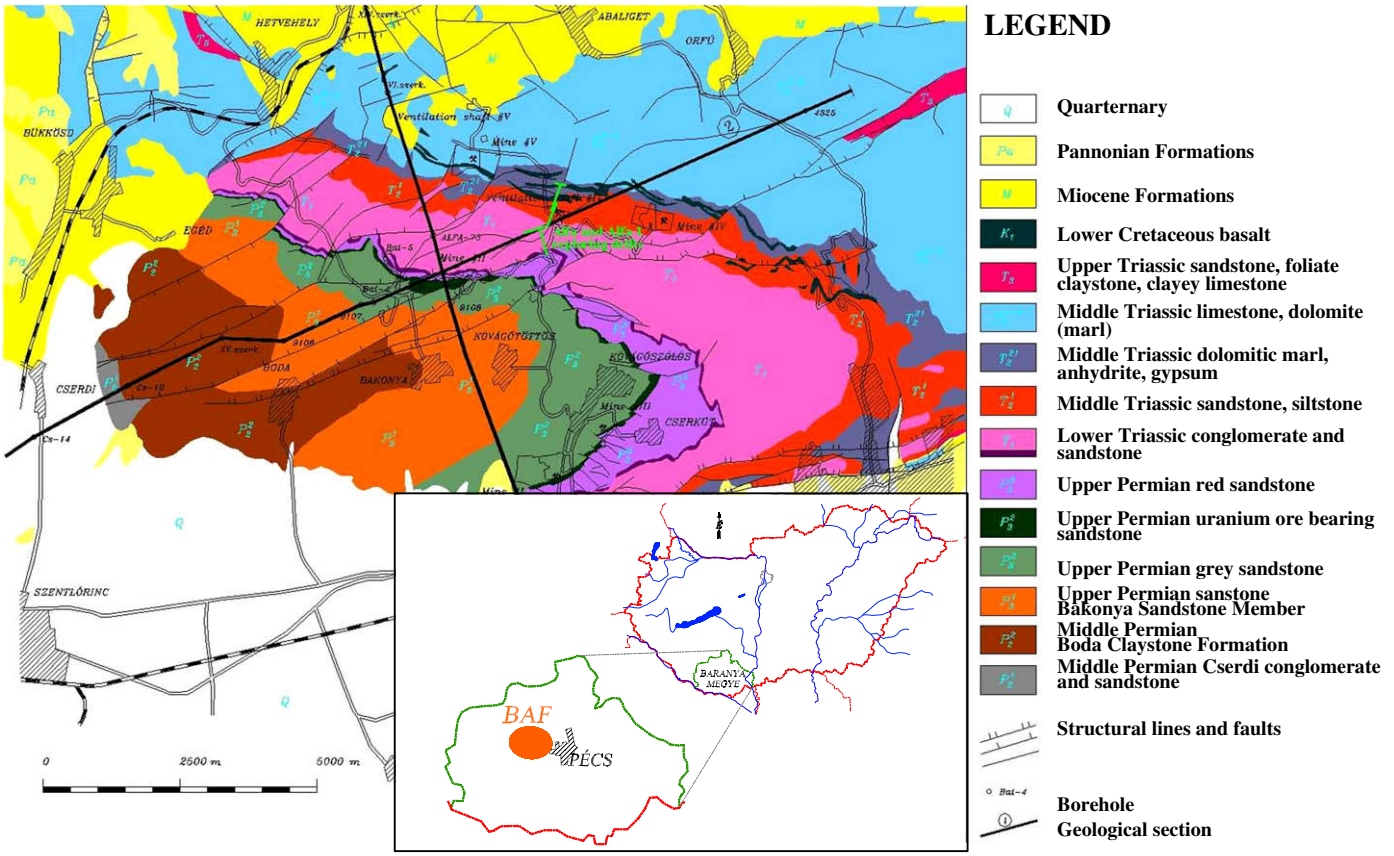
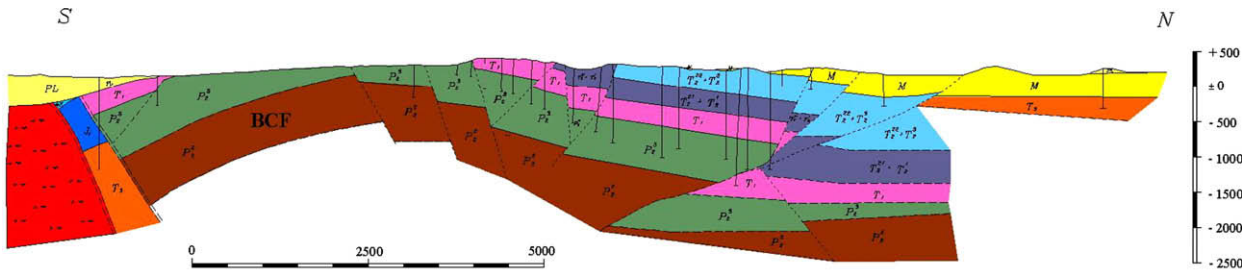


Fig. 1. Geological map of the Western-Mecsek Anticline with the location of URL and surface outcrop area of BCF (Kovács ed., 1999).



PL — Pannonian sediments (sand, clay, marl)

M — Miocene sediments (gravel, sand, marl)

J–K — Middle Jurassic, Cretaceous layers

J — Lower Jurassic layers

T_3 — Upper Triassic sandstone, foliate claystone, clayey limestone

T_2^{21}–T_2^{22} — Misina Formation Group Viganvár Limestone Member

T_2^{21}–T_1 — Aquiclude layers of Magyarürög Anhydrite Member Patacs Formation

T_1 — Jakabhegy Sandstone Formation

P_2^3 — Kővágószőlős Sandstone Formation with uranium bearing layers (sandstone, conglomerate)

P_2^2 — Boda Claystone Formation (claystone, siltstone with thin layers of dolomitic marl, dolomite

Crystalline (granitic rocks) basement

Structural lines, faults

Important borehole

Supposed boundary of formation

Fig. 2. Geological cross section of the Northern–Southern direction in the Western-Mecsek Anticline (Kovács ed., 1999).

In the early 1990s exploration shafts, the so-called Alfa and Alfa-1 Shaft was excavated in overall 1303 m length from the former uranium mine 1000 m underground (Fig. 3). The BCF was explored by 346 m length of tunnel, and by 70 underground

Author's personal copy

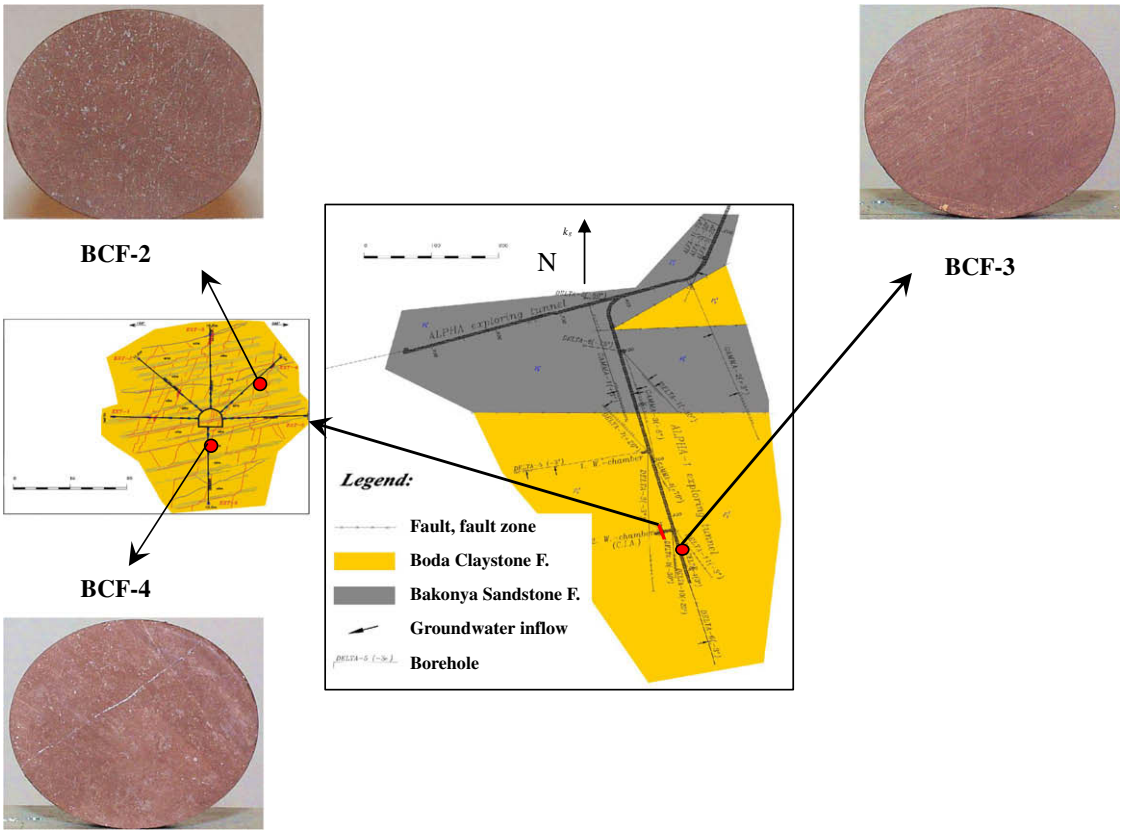


Fig. 3. The layout of URL with the exploring tunnels and boreholes (Kovács ed., 1999) sampling marked by red dots. (For interpretation of the references to colour in this figure legend, the reader is referred to the web version of this article.)

boreholes with overall 3810 m length (2300 m in BCF). This was one of the first and deepest URLs in the world to investigate argillaceous rocks.

During the operation of the URL, some in situ and laboratory measurements were executed to determine porosity (0.04–1.71% (SZKFI report, 1990, 1991), 0.64–1.53% (MÉV report, 1993), and 0.5–1.48% Csicsák (ed.), 1999) and permeability under stress and at a given temperature (1.713×10^{-17} m^2 in case of gas, Csicsák (ed), 1999; 10^{-15}–10^{-18} m^2 in case of water, SZKFI report, 1990, 1991). Only very limited in situ permeability measurement were carried out (BAT-4 and BAT-5 boreholes, Csicsák, personal information, 2007). On the basis of hydraulical tests primary influence of the microfractured character of BCF could be recognized on the rock physical parameters (Csicsák (ed), 1999).

The peculiar physical and chemical characteristics of the investigated rocks induced applying new methods and experimental developments, whereas the traditional methods, e.g. steady state flow test on the basis of Darcy's law, were unenforceable due to their non robustness, time-consuming character and the unreliability of results (Davy et al., 2007). One of the new methods used was the pressure pulse decay (PPD) technique to estimate gas and water permeability (Lakatos et al., 2002).

2. Methods and experiments

2.1. Sample preparation

Four core samples representing the dominant rock type (claystone) of BCF, from the underground borehole Delta-4 and the nearby extensometer boreholes (EXT-4, 6) of the Alfa shaft (Fig. 3.) were investigated in 2002 for their porosity, mercury porosimetry, and permeability and in 2007 for their geochemistry, mineralogy and mercury porosimetry.

At first, large cores were obtained by water-cooled diamond-saw blade. The sample BAF-1 was used determining the physical behaviour of rock during cutting, and BCF-2 to 4 samples served for determining the rock matrix density and the effective porosity by He-porosimetry (Quantachrome MVP-5 Multipycnometer and calculation, see in Results). The pycnometer was calibrated for different temperatures (29.4 °C (BCF-2) 21.7 °C (BCF-3 and BCF-4)). Parameters (volume) were calculated from 21 pair of measured values during the calibration and measurement. Due to its minimal uncertainty, the highest sample cell was used.

Next, gas and water permeability measurements were performed on small cores (BCF-2/1, BCF-2/2, BCF-3/2, BCF-3/3, BCF-4/2, BCF-4/3) in parallel with the entrance pore radius size distribution by mercury porosimetry (BCF-2/3, BCF-2/4). Geometrical sizes were measured by calliper statistically (6–11 different length measurements, and 5–7 different diameter measurements of each samples), and time dependence of drying of large and small samples are shown in Tables 1 and 2.

Due to the first results obtained by mercury porosimetry (Quantachrome 500 Medium Pressure Mercury Porosimeter), the second (BCF-2/4) measurement was not performed, and hence, this core data were eliminated from Table 2. In 2007, new samples were cut from old samples (BCF-3/4 and BCF-4/4) and high pressure mercury porosimetry (combination of Thermo Finnigan Pascal-140 (from 58,000 to 1900 nm pore throat size) and Pascal-440 (from 15000 to 3.6 nm pore throat size)) measurement were executed.

All the samples were dried at 105 °C to obtain the dry mass (Tables 1 and 2) before pycnometry, mercury porosimetry and

Author's personal copy

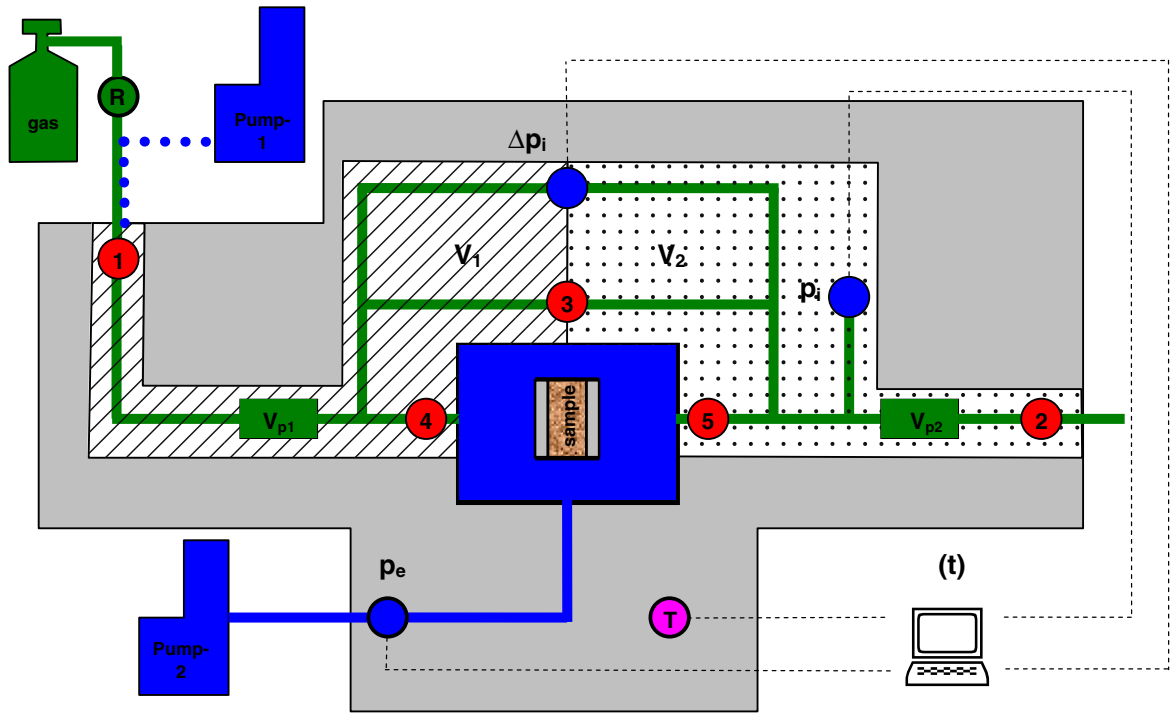
Table 1
Geometry and time of drying of large samples.

Sample ID	Sampling point	d (mm)	l (mm)	V (cm^3)	t (day)
BCF-2	EX-T-4/2: 9.2–9.29 m	36.30 ± 0.01	69.87 ± 0.04	72.31 ± 0.08	41
BCF-3	EX-T-6: 3.265–3.375 m	36.31 ± 0.01	69.36 ± 0.11	71.82 ± 0.15	37
BCF-4	Delta-4: 62.15–62.32 m	35.95 ± 0.01	69.47 ± 0.03	70.52 ± 0.11	41

Table 2
Geometry, initial (W_0) and dry weight (W_d) and time of drying of small samples.

Sample ID	d/a_1 (mm)	a_2 (mm)	l (mm)	V (cm^3)	W_0 (g)	W_d (g)	t (day)
BCF-2/1	36.290 ± 0.010	–	9.930 ± 0.000	10.271 ± 0.006	28.2066	27.9824	~10
BCF-2/2	36.284 ± 0.009	–	10.026 ± 0.005	10.367 ± 0.011	28.4567	28.2316	~8
BCF-2/3	6.803 ± 0.019	6.973 ± 0.025	32.933 ± 0.122	1.562 ± 0.016	4.2540	4.2195	~5
BCF-3/2	36.310 ± 0.007	–	10.133 ± 0.032	10.492 ± 0.037	28.3787	28.3630	~6
BCF-3/3	36.316 ± 0.005	–	9.929 ± 0.078	10.285 ± 0.084	27.7733	27.7609	~15
BCF-4/2	35.958 ± 0.015	–	10.381 ± 0.031	10.542 ± 0.040	28.4852	28.4347	~11
BCF-4/3	35.944 ± 0.017	–	9.974 ± 0.015	10.020 ± 0.025	27.1541	27.1068	~11

d is diameter, a_1, a_2 are lengths along sides of the bock (cubic sample).



Gas: N_2, or other gas (CO_2, He, Ar, CH_4); **Pump-1, Pump-2:** hydraulic pumps ; R : pressure regulator

Sample: sample in Hassler-type core holder; **p_e:** hydrostatic confining pressure; T: temperature

Δp_i: differential pressure transducer; **p_i**: pressure transmitter; **1,2** :needle valves; **3,4,5:** valves ; t: time

V_{p1}, V_{p2} : reservoirs

heat controlled area

components of V_1 upstream volume

components of V_2 downstream volume

High-pressure core holder

Fig. 4. Schematic figure of measurement system.

Author's personal copy

gas permeability measurements. However, the dried samples have absorbed very quickly the humidity of the atmosphere. Then, it was necessary to keep them under vacuum during cooling (2–4 h) and after in exsiccator. The measurement of dried mass on cooled state cores was executed with a high precision analytical scale (10^{-3} g accuracy).

The water permeability measurements were carried out on fully saturated small samples by distillated water. The samples' mass was also measured with the same accurate scale.

Before each measurement, all cores were digitally documented by video and high resolution picture.

2.2. Mercury porosimetry

The theoretical basis of this measurement is that the pore radius is inversely proportional to the applied pressure according to the relation proposed by Washburn (Lowell et al., 1991):

$$r = \frac{2\sigma_{Hg}\cos\theta_{Hg}}{p} \quad (1)$$

where r is the radius of pores (m), σ_{Hg} is the interfacial tension of mercury (480 mN/m during these measurements), θ_{Hg} is the contact angle (141.3° during these measurements); p the absolute applied pressure (Pa).

The Thermo Finnigan PASCAL 140 and PASCAL 440 type mercury porosimeter equipments applied to inject mercury into the samples for pressures up to 400 MPa (pore size measurement from 4 nm (4×10^{-9} m for p = 400 MPa) up to 200 μm (200×10^{-6} m for p = 0.01 kPa). The mercury porosity and the pore-throat size distribution were determined with this equipment and the following parameters were calculated from these results.

Total specific cumulative volume (cm^3/g): total volume of mercury having penetrated into the sample at the end of measurement (V_{cum}).

Total specific surface area (m^2/g): total surface of the pores calculated on the basis of the given geometrical model (SA_{spec}). Due to the differences in theory and the limitations of the measurement the calculated parameter cannot generally be compared to surface areas measured by gas adsorption experiments (BET). In this case the Conical Model was used.

Bulk density (g/cm^3): the density of the sample referred to its geometrical volume (ρ_{bulk}).

Apparent density (g/cm^3): the density of the sample referring to the real sample volume (excluding therefore the volume of pores and inter-particle voids) (ρ_{app}).

Total porosity (%): pore volume to total apparent volume (Φ_{Hg}).

2.3. PPD permeability measurement

The main advantage of the PPD permeability compared with traditional permeability measurements is that very fast experiments can be performed (in case of $k_g \sim 10^{-19}$ m^2 15–25 min, $k_w \sim 10^{-21}$ m^2 6–7 h), under limited pressure difference (only 0.1–0.5 MPa) applied at the two sides of the examined core. Another advantage is that quasi in situ circumstances can be provided and that the measurement uncertainly can be estimated.

The principle of the measurement is that the time of pressure pulse decay between the two sides of a core depends on the permeability of the rock. Theoretical background is given by many articles, e.g. Dicker and Smits (1988), Jones (1997). The aim was to investigate cores in quasi reservoir conditions (35 °C, 6–7 MPa, N_2 gas/distilled water) in a relatively short time and to estimate the uncertainty of the results. The geometry of the system is shown in Fig. 4. The hugest advantage of the measurement, and this is the reason why it is so fast, is that it does not need to measure quantitatively the gas or fluid flow.

During the measurement, following a short transient period, the pressure pulse decay becomes exponential beside the stochastic noise. If all simplifications are applied like symmetrical setting (equal upstream (V_1) and downstream (V_2) volumes) and an internal volume ($V_1 + V_2$) not to big in comparison to the pore volume, then the later phase of flooding uses a basic equation based on the dimensionless pressure difference dependence of dimensionless time (Dicker and Smits, 1988) becomes easier (Jones, 1997). In case of gases, it finally gives:

$$\ln[\Delta p_D] = \ln[f_0] - m \cdot t = \ln[f_0] - \left[\frac{k_g \cdot \theta_1^2}{(c_g + c_{pv}) \cdot \mu_g \cdot \Phi \cdot L^2}\right] \cdot t \quad (2)$$

where Δp_D is pressure difference (dimensionless), f_0 is constant depending on the pore and internal volumes and on the gas compressibility (dimensionless), m is slope (1/s), t is relative time compare to the measurement starting time (t_0) (s), k_g is gas permeability (m^2), θ_1 is constant depending on the pore and internal volumes, and on the gas compressibility (dimensionless), c_g is gas compressibility at a given temperature and pressure (1/Pa), c_{pv} is compressibility of the total pore volume (1/Pa), μ_g is gas viscosity at a given temperature and pressure (Pa s), Φ is porosity (dimensionless), L is sample length (m).

In a log pressure difference ($\ln(\Delta p_D)$) versus time plot a linear trend can be obtained and provide f_0 (in fact f_0 at the intersection of the X axis) and m the (line's slope).

The gas permeability (k_g) can be calculated from the following equation:

$$k_g = \frac{|m| \cdot \mu_g \cdot L \cdot f_z}{f_1 \cdot A \cdot \left(\frac{1}{V_1} + \frac{1}{V_2}\right)} \quad (3)$$

where A is cross section area of sample (m^2), V_1, V_2 is upstream and downstream volumes $V_1 = V_2$ (m^3), f_0 is constant, depends on the pore volume, internal volume and compressibility of gas, pores and internal volumes (dimensionless).

The water permeability could be calculated from the following equation:

$$k_L = \frac{|m| \cdot \mu_w \cdot L \cdot (c_w + c_{V_1})}{f_1 \cdot A \cdot \left(\frac{1}{V_1} + \frac{1}{V_2}\right)}, \quad (4)$$

where c_w is the effective compressibility of the water, which could be estimated from a correlation of Meehan (1980) (1/Pa), c_{V1} is compressibility of the upstream volume, constant (1/Pa), μ_w is water viscosity as a function of T, p and salt concentration, estimated on the basis of Numbere et al. (1977) (Pa s).

Both equations can be applied regarding to the facts that:

- The compressibility of the internal volume is negligible compared to the gas compressibility.
- The pore volume (V_p) can be calculated from the sample geometry and porosity.
- The c_g can be calculated as a ratio of modified Z factor (f_z) and pore pressure (p), where f_z can be calculated indirectly from the Beattie–Bridgeman state equation applied for realistic gases.
- The μ_g can be calculated from the formula reported in Lee et al. (1966).
- The absolute value of slope can be estimated from the $\ln(\Delta_{PD})$ versus time plot.

Either in case of gas or water, the slope of the line can be calculated for a given time period. It means that the permeability values may be calculated for "$n-1$" case if the all measured point is "n". The uncertainty of permeabilities can only be estimated for the exponential period. It was possible to identify measurement prob-

Author's personal copy

lems by comparing the two different calculations based either on the slope of the fitted line (k_{g3}, k_{w3}) or by statistical way from single point values (k_{g2}, k_{w2}). Problems coming from pressure dependence of physico-chemical and physical parameters are negligible by using low pressure difference.

A new experimental PPD permeameter was built to measure both gas and water permeability. During the measurement several parameters were detected automatically like the relative time (s), the external hydrostatical pressure (p_e (bar)), the pressure difference between the two sides of the sample (Δp (bar), up to 5 bar), the downstream pressure (p_i (bar) up to 200 bar) and the temperature of the Hassler-type core holder (T [°C]). Time steps were regulated between 400 and 5000 ms. Each detection is the average of 200 measured values. The external pressure must be 15–30 bar higher than the downstream pressure (p_i). Thus, the cotton sheath surrounding the sample airtights and hence, the flow can only happen across the rock. The internal volume on the two sides of the sample are equals (Fig. 4) and about 100 times higher than the pore volume of the sample. Because of the lack of thermostat, a small room was heated up to 40 °C and the air was circulated regularly, thus the temperature variation during the experience was less then 0.3–0.5 °C.

Data processing and interpretation was carried out on Excel sheet using macros. All the different units used for calculation were converted to SI units. Running median was calculated for each 100 Δp and p_i values, thus decreasing the noise. The positive and 0 values of slope were filtered and eliminated. Slopes and all different parameters were calculated after filtering at a given moment, and hence, the k_g values ($k_{g\text{-}1}$, $k_{w\text{-}1}$) were calculated. The line slope is defined as follows:

$$\frac{1}{200}\sum_{n=i}^{i+200}(m_n - m_{n-1}) = 0 \pm 10^{-10} \quad (5)$$

The first moment, when Eq. 5 is satisfied, is the start point for the k_{g-1} calculation. Then, the median, mean and standard deviation for the full range of k_{g-1} was calculated (k_{g-2}). It is comparable with the calculated k_g value determined from the graphical fitting slope (k_{g-3}).

In case of water permeability, the strongly monotonic decrease of Δp is required. The different k_w values were calculated in the same way as for gas permeabilities (k_{w-1}, k_{w-2}, k_{w-3}), but uncertainty was much higher for samples not fully saturated. Hence, the median and mean of the last 100 k_{w-1} values, as k'_{w-2} were applied during interpretation.

Gas permeability was measured by using N_2 gas. N_2 absorption was eliminated due to the lack of organic compounds. The downstream pressures were corrected with a blank pressure measurement at a given temperature. The average pressure (p_{mean}) was defined as the sum $\Delta p + p_i$ devided by the number of p_i measurements. The reproducibility of measurements in the sample BCF-2/2 was also examined.

Before the water permeability measurement, the system was saturated with distilled water. For still unknown reasons, the saturation of cores was not fully successful. Therefore, it was assumed that the first period the experiment corresponded to the core saturation.

The system was very sensitive to temperature changes and pressure fluctuations.

2.4. Geochemical and minerological analysis

Geochemical analysis were performed in 2007 at the QUALITEST LABORATORY Ltd. with a ARL 8410 type sequential X-ray fluorescence spectrometer. The mineralogical composition was obtained by the Geochemical Research Institute of Hungarian Academy of Science using a PHILIPS PW 1730 type Bragg–Brentano scheme diffractometer. Microscopical studies were carried out at the Mineralogical and Petrological Laboratory of MECSEKÉRC Ltd.

3. Results and interpretation

The main goal of this article was to apply and modify (applying higher temperature, modified data processing) a technique already used in the hydrocarbon exploration for permeability measurements of very tight rocks and modify it in order to make it applicable at a larger scale as only the full scale geochemical, mineralogical, petrophysical and hydrogeological examination can help to understand the behaviour of the BCF in the case of HLW research purpose.

3.1. Sample preparation

During cutting some sample (BCF-3/1, BCF-4/1) were destroyed because of the fracturing along tectonic microfissures or damaged structures. The microfissures were evidenced during wet cutting and could not be recognized in other way. Those microfissures damaged of the main part of the BCF-4 sample. In other samples, small irregular slips were recognized (BCF-4/1).

3.2. Porosity measurement

Samples originated from BCF have an exceptionally low porosity (maximum 3%), therefore it cannot be calculated by using He-pycnometry. At the previously determined gas permeability values by traditional permeametry (10^{-16}–10^{-18} m^2) (SZTAKI reports,1990, 1991, MÉV report, 1993; Csicsák (ed), 1999), the flow time of He is too long at low pressure (0.17 MPa) and during this time the pressure and temperature can be changed. The accuracy of the measurement was only 10^{-1} cm^3 for large samples. This value must be compared to the pore volume (1–3 cm^3).

Because of this, a new way had to be found to decrease the uncertainty of about one order of magnitude. For practical reason, it was better to use homogeneous and large samples. Very small porosities were determined on fully saturated samples by measuring the sample volumes by He-pycnometry (BCF-2, BCF-3, BCF-4). Therefore, compared to the geometrical volume measured by calliper and its associated error, these values are assumed to give the initial "porosity" and their extreme values (Table 3).

Samples were dried at atmospheric pressure (p_{atm}), the experimental rock temperature (T_{rock}), and the brine concentration are those of the existing literature (1–7 g/l, MÉV, 1993; Csicsák (ed), 1999). The volume of water (V_w) evaporated during drying was cal-

Table 3
Initial "porosity" values measured in wet cores.

Sample ID	Time of measurement	T_{atm} (°C)	T_{calib} (°C)	W_0 (g)	ρ_{bulk} (g/cm^3)	$V_{measured}$ mean (cm^3)	$V_{measured}$ median (cm^3)	Φ_{mean} (%)	$\Phi_{abs\text{-}max}$ (%)
BCF-2	2002.07.08	29.4	29.4	198.3429	2.745 ± 0.003	72.26 ± 0.08	72.28	0.04	0.32
BCF-3	2002.09.17	21.7–22.0	21.7	196.3869	2.737 ± 0.001	71.76 ± 0.04	71.77	0.08	0.38
BCF-4	2002.09.18	21.3–21.4	21.7	192.8664	2.740 ± 0.001	70.40 ± 0.02	70.40	0.17	0.53

Author's personal copy

Table 4
Calculated matrix density (ρ_{calc}), matrix volume ($V_{matrix\text{-}calc}$) and porosity (Φ_{med}) after drying.

Sample ID	Time of measurement	T_{atm} (°C)	T_{rock} (°C)	W_{dry} (g)	ρ_{calc} (g/cm^3)	$V_{matrix\text{-}calc}$ (cm^3)	Φ_{med} (%)
BCF-2	2002.08.28.	27.4	27.4	196.8440	2.780 ± 0.005	70.809	2.07
BCF-3	2002.10.25.	23.5	30.0	195.6180	2.753 ± 0.007	71.403	1.08
BCF-4	2002.10.28.	25.7	25.7	191.3259	2.774 ± 0.005	68.975	2.18

Table 5
Results of mercury porosimetry (r_{mean} is the average entrance pore radius).

Sample ID	Time of measurement	W_{dry} (g)	ρ_{app} (g/cm^3)	V_{cum} (cm^3/g)	SA_{spec} (m^2/g)	Φ_{Hg} (%)	r_{mean} (μm)
BCF-3/4	2007.07.11.	5.0826	2.722	0.0012	0.149	0.315	0.004
BCF-4/4	2007.07.11.	4.6835	2.709	0.0022	0.344	0.604	5.823

culated as the ratio of the difference between the initial and the dry mass and the brine density. The errors estimated at the different salt concentration (applied 7 g/l) and the differences between T_{rock} and T_{atm} are negligible. The effective porosity values were calculated by taking into account V_w from $V_{geometrical}$, the volume of matrix, and thus, the matrix density.

Due to the homogeneity of the large samples, the porosity and matrix density values of small samples were calculated on the basis of results reported in Table 4.

3.3. Mercury porosimetry

The measurements of mercury porosimetry had to be repeated with a high pressure mercury porosimeter because on the basis of first measurement performed in 2002. New measurements indicate that more than three-quarter of pores are lower mezopores and micropores. Due to the lack of sample BCF-2, samples were only repeated for BCF-3 and BCF-4. The results are shown in Table 5.

In case of BCF-3/4 the ρ_{app} and Φ_{Hg} values indicate that the sample was not completely dried or that some water was produced by illite. The assumed very low pore radius (4–20 nm) is proved to be true.

Alike previous sample, the measurement of BCF-4/4 gave similar results with a first family ranging between 4 and 15 nm. Besides the 4–15 nm pore radius, the other range could be recognized between 5–7 μm. It seems that some microfractures initially filled with carbonates (see for instance in Fig. 5) were opened at a given pressure.

3.4. PPD permeability

Results of gas permeability measurements are shown in Table 6. However, this table does not contains the individual k_g and k_w values, k_{g-1} and k_{w-1}, respectively. Alone the estimates of extremes (the $k_{abs-max}$ and $k_{abs-min}$) were allowed. The calculated gas permeabilities are 10^{-18}–10^{-19} m^2. The heterogeneity of permeability can be seen by comparing BCF-2/1 and BCF-2/2, as well as BCF-3/2 and BCF-3/3. A decreasing trend in gas permeability values is observed when T and p_e are nearly constants and p_{mean} decreases. In the future this trend should be investigated in more details. The best parameter is likely the k_g median values (k_{g-med}) due to its robust character, i.e. less sensitive to data filtering and data loss. However, in most cases the difference between calculated parameters ($k_{g-2\ med}$, $k_{g-2\ átlag}$, k_{g-3}) is negligible.

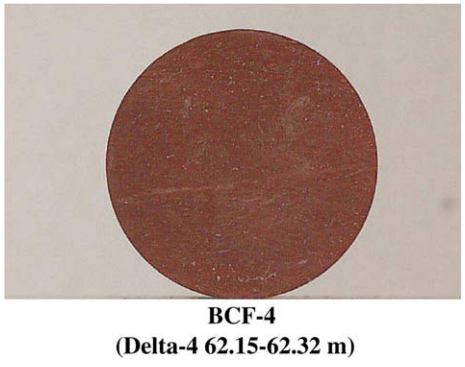


Fig. 5. The BCF-4 sample with a microfissure in the mid part of the picture.

Water permeability values are reported in Table 7. During the measurements lot of questions emerged which are in connection with the mineralogical composition of the BCF. The sensitivity of the saturated system caused problems on absolute pressure measurements. It seems important to study the fluctuations of pressure difference between the hydrostatic pressure and pore pressure to the calculated k_w values.

Another problem was that the mass of the saturated sample more or less increased during the measurement. At constant T and p_e, p_i decreased continuously with very low decreasing of Δp and increasing k_w in BCF-4/3. It means, that the saturation process was not achieved, and hence, the uncertainty of this result is very big. It seems that the mean of last 100 k_w values is the best approach. When the core is fully saturated, p_i is increasing and Δp is decreasing continuously. The weight difference between the initial and final state of measurement was +0.2475 g water in case of the BCF-4/3 sample. The difference of BCF-3/3 and BCF-2/2 samples was much lower, 0.0994 g and 0.0453 g, respectively.

3.5. Geochemical and minerological analyses

Full geochemical and mineralogical analysis were performed in 2007 to check whether or not the observed phenomena during the helium and mercury porosimetry as well as during the water permeability measurements are due to the relatively high water saturated phyllosilicate content.

On the basis of minerological analysis, all of the samples are strongly albitic claystone (Table 8). Main mineral is the authgenous albite (46–49%) as an albitic cement and less common as albitic nests. The low quartz content is typical of an albitolite. The quantity of hematite is approximately. Two times higher than in a common albitolite and also higher of the average value in claystone. The main clay mineral is the 10 Å phyllosilicate (illite-muscovite). Minor chlorite and no smectite were determined. The carbonatic content is manifold. A low quantity of orthoclase also was detected.

The same rock types has relatively uniform chemical character on the basis of high amount of previous analyses (Máthé, 1998; Árkai et al., 2000; Varga et al., 2005, 2006). Compared to the

Author's personal copy

Table 6
Gas permeability results.

sample ID	T (°C)	p_{mean} (MPa)	$p_e - p_i$ (MPa)	$k_{g\text{-}2med}$ (m^2)	$k_{g\text{-}2mean}$ (m^2)	σ (+/−)	$k_{g\text{-}3}$ (m^2)	ABS ($k_{g\text{-}2} - k_{g\text{-}3}$)
BCF-2/1	35.78 ± 0.05	7.95	2.93 ± 0.03	$6.66 \cdot 10^{-19}$	$6.59 \cdot 10^{-19}$	$1.6 \cdot 10^{-20}$	$6.54 \cdot 10^{-19}$	$0.12 \cdot 10^{-19}$
BCF-2/1	34.60 ± 0.12	6.84	2.15 ± 0.03	$7.18 \cdot 10^{-19}$	$7.12 \cdot 10^{-19}$	$1.8 \cdot 10^{-20}$	$7.14 \cdot 10^{-19}$	$0.04 \cdot 10^{-19}$
BCF-2/1	35.51 ± 0.11	6.80	2.49 ± 0.02	$6.56 \cdot 10^{-19}$	$6.55 \cdot 10^{-19}$	$1.9 \cdot 10^{-20}$	$6.68 \cdot 10^{-19}$	$0.12 \cdot 10^{-19}$
BCF-2/1	34.56 ± 0.05	5.83	1.61 ± 0.03	$7.44 \cdot 10^{-19}$	$7.55 \cdot 10^{-19}$	$2.8 \cdot 10^{-20}$	$7.43 \cdot 10^{-19}$	$0.01 \cdot 10^{-19}$
BCF-2/1	34.25 ± 0.07	5.77	1.64 ± 0.02	$7.15 \cdot 10^{-19}$	$7.13 \cdot 10^{-19}$	$1.4 \cdot 10^{-20}$	$7.30 \cdot 10^{-19}$	$0.15 \cdot 10^{-19}$
BCF-2/1	33.87 ± 0.05	4.84	1.73 ± 0.02	$6.87 \cdot 10^{-19}$	$6.84 \cdot 10^{-19}$	$1.3 \cdot 10^{-20}$	$7.10 \cdot 10^{-19}$	$0.23 \cdot 10^{-19}$
BCF-2/1	33.98 ± 0.08	4.76	1.75 ± 0.03	$7.04 \cdot 10^{-19}$	$7.05 \cdot 10^{-19}$	$1.7 \cdot 10^{-20}$	$7.04 \cdot 10^{-19}$	$0.00 \cdot 10^{-19}$
BCF-2/2	34.47 ± 0.07	8.07	2.10 ± 0.03	$1.33 \cdot 10^{-19}$	$1.33 \cdot 10^{-19}$	$3.1 \cdot 10^{-21}$	$1.32 \cdot 10^{-19}$	$0.01 \cdot 10^{-19}$
BCF-2/2	34.49 ± 0.06	7.99	2.16 ± 0.02	$1.34 \cdot 10^{-19}$	$1.34 \cdot 10^{-19}$	$2.1 \cdot 10^{-21}$	$1.34 \cdot 10^{-19}$	$0.00 \cdot 10^{-19}$
BCF-2/2	34.30 ± 0.06	6.98	2.10 ± 0.03	$1.26 \cdot 10^{-19}$	$1.26 \cdot 10^{-19}$	$3.0 \cdot 10^{-21}$	$1.27 \cdot 10^{-19}$	$0.01 \cdot 10^{-19}$
BCF-2/2	34.83 ± 0.06	6.90	2.10 ± 0.03	$1.28 \cdot 10^{-19}$	$1.29 \cdot 10^{-19}$	$2.9 \cdot 10^{-21}$	$1.29 \cdot 10^{-19}$	$0.01 \cdot 10^{-19}$
BCF-2/2	34.72 ± 0.07	5.84	2.09 ± 0.02	$1.24 \cdot 10^{-19}$	$1.24 \cdot 10^{-19}$	$3.0 \cdot 10^{-21}$	$1.24 \cdot 10^{-19}$	$0.00 \cdot 10^{-19}$
BCF-2/2	34.61 ± 0.03	4.93	2.11 ± 0.02	$1.20 \cdot 10^{-19}$	$1.20 \cdot 10^{-19}$	$2.5 \cdot 10^{-21}$	$1.21 \cdot 10^{-19}$	$0.01 \cdot 10^{-19}$
BCF-2/2	34.60 ± 0.03	3.90	2.15 ± 0.02	$1.17 \cdot 10^{-19}$	$1.17 \cdot 10^{-19}$	$3.2 \cdot 10^{-21}$	$1.17 \cdot 10^{-19}$	$0.00 \cdot 10^{-19}$
BCF-3/2	35.48 ± 0.04	7.97	2.01 ± 0.03	$1.51 \cdot 10^{-18}$	$1.52 \cdot 10^{-18}$	$3.5 \cdot 10^{-20}$	$1.56 \cdot 10^{-18}$	$0.05 \cdot 10^{-18}$
BCF-3/2	35.40 ± 0.00	7.90	1.98 ± 0.02	$1.58 \cdot 10^{-18}$	$1.59 \cdot 10^{-18}$	$3.1 \cdot 10^{-20}$	$1.59 \cdot 10^{-18}$	$0.01 \cdot 10^{-18}$
BCF-3/2	35.48 ± 0.04	6.94	1.98 ± 0.02	$1.53 \cdot 10^{-18}$	$1.54 \cdot 10^{-18}$	$7.2 \cdot 10^{-20}$	$1.53 \cdot 10^{-18}$	$0.00 \cdot 10^{-18}$
BCF-3/2	35.44 ± 0.07	5.93	1.92 ± 0.02	$1.46 \cdot 10^{-18}$	$1.46 \cdot 10^{-18}$	$3.8 \cdot 10^{-20}$	$1.46 \cdot 10^{-18}$	$0.00 \cdot 10^{-18}$
BCF-3/2	35.44 ± 0.06	4.94	1.99 ± 0.02	$1.34 \cdot 10^{-18}$	$1.35 \cdot 10^{-18}$	$5.3 \cdot 10^{-20}$	$1.33 \cdot 10^{-18}$	$0.01 \cdot 10^{-18}$
BCF-3/2	35.31 ± 0.07	3.95	2.06 ± 0.02	$1.18 \cdot 10^{-18}$	$1.19 \cdot 10^{-18}$	$1.5 \cdot 10^{-20}$	$1.21 \cdot 10^{-18}$	$0.03 \cdot 10^{-18}$
BCF-3/3	35.20 ± 0.04	7.93	2.06 ± 0.03	$7.93 \cdot 10^{-19}$	$8.06 \cdot 10^{-19}$	$2.7 \cdot 10^{-20}$	$8.20 \cdot 10^{-19}$	$0.27 \cdot 10^{-19}$
BCF-3/3	35.09 ± 0.03	7.88	2.06 ± 0.03	$7.79 \cdot 10^{-19}$	$7.85 \cdot 10^{-19}$	$1.2 \cdot 10^{-20}$	$7.78 \cdot 10^{-19}$	$0.01 \cdot 10^{-19}$
BCF-3/3	34.96 ± 0.06	6.93	1.93 ± 0.03	$7.20 \cdot 10^{-19}$	$7.18 \cdot 10^{-19}$	$1.3 \cdot 10^{-20}$	$7.45 \cdot 10^{-19}$	$0.25 \cdot 10^{-19}$
BCF-3/3	34.99 ± 0.02	5.95	1.96 ± 0.03	$7.04 \cdot 10^{-19}$	$7.06 \cdot 10^{-19}$	$2.7 \cdot 10^{-20}$	$7.00 \cdot 10^{-19}$	$0.04 \cdot 10^{-19}$
BCF-3/3	34.89 ± 0.05	4.93	1.97 ± 0.02	$6.74 \cdot 10^{-19}$	$6.72 \cdot 10^{-19}$	$1.3 \cdot 10^{-20}$	$6.68 \cdot 10^{-19}$	$0.06 \cdot 10^{-19}$
BCF-4/2	35.20 ± 0.02	7.93	2.03 ± 0.03	$1.02 \cdot 10^{-18}$	$1.03 \cdot 10^{-18}$	$3.1 \cdot 10^{-20}$	$1.04 \cdot 10^{-18}$	$0.02 \cdot 10^{-18}$
BCF-4/2	34.95 ± 0.07	6.88	2.09 ± 0.02	$9.51 \cdot 10^{-19}$	$9.53 \cdot 10^{-19}$	$2.0 \cdot 10^{-20}$	$9.51 \cdot 10^{-19}$	$0.00 \cdot 10^{-19}$
BCF-4/2	34.83 ± 0.04	5.94	2.11 ± 0.03	$8.98 \cdot 10^{-19}$	$8.93 \cdot 10^{-19}$	$1.7 \cdot 10^{-20}$	$8.96 \cdot 10^{-19}$	$0.02 \cdot 10^{-19}$
BCF-4/2	34.70 ± 0.06	4.97	2.05 ± 0.03	$8.79 \cdot 10^{-19}$	$8.77 \cdot 10^{-19}$	$1.9 \cdot 10^{-20}$	$8.69 \cdot 10^{-19}$	$0.10 \cdot 10^{-19}$
BCF-4/2	35.00 ± 0.11	4.05	2.06 ± 0.02	$8.16 \cdot 10^{-19}$	$8.10 \cdot 10^{-19}$	$2.7 \cdot 10^{-20}$	$8.20 \cdot 10^{-19}$	$0.04 \cdot 10^{-19}$
BCF-4/3	35.31 ± 0.04	7.98	2.06 ± 0.02	$1.49 \cdot 10^{-18}$	$1.49 \cdot 10^{-18}$	$6.3 \cdot 10^{-20}$	$1.51 \cdot 10^{-18}$	$0.02 \cdot 10^{-18}$
BCF-4/3	35.39 ± 0.04	6.94	2.11 ± 0.03	$1.35 \cdot 10^{-18}$	$1.37 \cdot 10^{-18}$	$5.1 \cdot 10^{-20}$	$1.37 \cdot 10^{-18}$	$0.02 \cdot 10^{-18}$
BCF-4/3	35.23 ± 0.06	5.96	2.09 ± 0.03	$1.28 \cdot 10^{-18}$	$1.28 \cdot 10^{-18}$	$1.5 \cdot 10^{-20}$	$1.28 \cdot 10^{-18}$	$0.00 \cdot 10^{-18}$
BCF-4/3	35.28 ± 0.06	4.96	2.09 ± 0.02	$1.25 \cdot 10^{-18}$	$1.24 \cdot 10^{-18}$	$3.9 \cdot 10^{-20}$	$1.26 \cdot 10^{-18}$	$0.01 \cdot 10^{-18}$
BCF-4/3	35.21 ± 0.05	3.89	2.14 ± 0.03	$1.25 \cdot 10^{-18}$	$1.26 \cdot 10^{-18}$	$2.2 \cdot 10^{-20}$	$1.22 \cdot 10^{-18}$	$0.03 \cdot 10^{-18}$

Table 7
Revised water permeability results.

Sample ID	T (°C)	p_{mean} (MPa)	$p_e - p_i$ (MPa)	k_{w-2med}* (m^2)	$k_{w-2mean}$* (m^2)	σ (+/−)	$k_{w\text{-}3}$ (m^2)	ABS ($k_{w-2\ med} - k_{w-3}$)
BCF-2/2	35.00 ± 0.09	6.95	2.23 ± 0.07	$1.55 \cdot 10^{-20}$	$1.60 \cdot 10^{-20}$	$1.5 \cdot 10^{-21}$	$1.13 \cdot 10^{-20}$	$0.42 \cdot 10^{-20}$
BCF-3/3	35.82 ± 0.06	6.92	3.04 ± 0.07	$3.66 \cdot 10^{-21}$	$3.68 \cdot 10^{-21}$	$8.7 \cdot 10^{-23}$	$2.50 \cdot 10^{-21}$	$1.11 \cdot 10^{-21}$
BCF-4/3	36.00 ± 0.01	6.43	3.20 ± 0.21	$1.61 \cdot 10^{-20}$	$1.62 \cdot 10^{-20}$	$6.2 \cdot 10^{-22}$	$2.81 \cdot 10^{-21}$	$13.29 \cdot 10^{-21}$

* The median and mean of the last 100 calculation.

Table 8
Minerological composition of the main rocks compared to the samples.

Rock type	Quartz (%)	Albite (%)	Clay minerals (%)		Carbonates (%)		Hematite (%)
			Illite-muscovite	Chlorite	Calcite	Dolomite	
Mineralogical composition of the characteristic rocks of BCF							
Albitic claystone	<15	25–40	35–50		5–15		7–15
Albitolite	<10	>50	<20		~10		5–7
Aleurolite	20–30	35–40	10–15		10–15		~5
Dolomite	<10	30–40	10–15		40–50		<5
Mineralogical composition of samples							
BCF-2	4	49	15	4	8	6	12
BCF-3	3	46	17	4	9	5	14
BCF-4	4	47	16	4	6	9	14

geochemical analysis of shale standard (Post-Archean Australian Average Shale – PAAS, Taylor and McLennan 1985; McLennan, 2001) the following differences can be recognised between claystones and albitolites:

– Corresponding to the mineralogical composition, within the claystones the depleted amount of SiO_2 and TiO_2, less concentration of Fe_2O_3, and more concentration of MgO, CaO, Na_2O, P_2O_5 can be observed.

Author's personal copy

- Concentration of MnO changes in high amounts, the Na_2O less and the K_2O is more concentrated (Varga et al., 2005; Varga et al., 2006).
- The concentration of Rb, Th, U, Y, Sc, Co, Zn, Pb are higher (in reductive layers, the U concentrated much higher), the Ba, Sr, Zr V, Ni are lower, while the amount of Cr, Hf, Nb, Ta are similar (Varga et al., 2006).
- Enrichment in SiO_2 is not observed in albitolites contrary to small enrichments in P_2O_5, Fe_2O_3, MgO and bigger enrichment in MnO, CaO and Na_2O (Varga et al., 2006).
- Because of the diagenetic alteration, the SiO_2 and Na_2O content of albitolites, aleurolites and sandstones are the highest with enrichment of CaO, MnO, Sr and Ba contents.
- The claystones are enriched in phyllosilicates and hematites with extreme amounts of Al_2O_3, Fe_2O_3, MgO, K_2O and Rb (Varga et al., 2006).

The chemical composition of the samples are similar to the higher albitic and carbonate content claystones. The concentration of tracers (Th, U, Zr, Hf, Nb, Ta, Y, V, Co, Ni, Zn) also show similarity to claystones except the Rb, which is depleted in two samples compared to the average claystones. This is due to the less illite content. Geochemical and mineralogical results suggest that no characteristic change in elemental and minerological composition happened.

4. Conclusions

On the basis of petrophysical and mineralogical, geochemical analysis the following conclusions can be drawn:

- The calculation of matrix porosity deduced from water content – using the weight differences of wet and dry state of the core and the geometrical core size – gives the only reliable information (compare the results of Table 3 and 4). The porosity is 1–3%, which is marginally higher than it was estimated previously. The time-consumption of drying and the fact that the dry core absorbs very fast the atmospheric humidity drew attention to the importance of the necessity of a careful preparation and handling as well as the necessity of geochemical and mineralogical analyses.
- Laboratory permeability measurements performed under reservoir condition show that the constant pressure difference (20–25 bar) between the outside and inside of rubber of Hassler-type core-holder and the constant temperature are very important.
- The gas and water permeabilities lower than measured before with extremes 10^{-18}–10^{-21} m^2 and 10^{-20}–10^{-23} m^2 respectively.
- A gas permeability decrease trend was observed at constant temperature in relationship with the internal pressure decrease. The latter has to be studied in more detail because not all reasons of the decrease are clearly defined.
- Water permeability values are approximately two orders of magnitude smaller than gas permeability values. During the water permeability measurements in quasi reservoir conditions ($p_i \approx 8$ MPa, $p_k \approx 10$ 12 MPa, $T \approx 36$ °C) the initial weight of saturated cores increased. The reasons of this phenomenon may be explained by the fact that (i) the saturation process during the experiment was not achieved and (ii) also to the mineralogical composition.
- On the basis of all results, the inhomogenity of permeability might be recognized.

The latter three dots have to be analysed in more details. The mineralogical composition, and thus, the behaviour of claystones and albitolites during drying and saturation is very important, because the effect of temperature and of atmospheric humidity in a repository are not negligible.

References

Árkai, P., Balogh, K., Demény, A., Fórizs, I., Nagy, G., Máthé, Z., 2000. Composition, diagenetic and post-diagenetic alterations of a possible radioactive waste repository site: the Boda Albitic Claystone Formation, Southern Hungary. Acta Geologica Hungarica vol. 43/4, 351–378.

Csicsák, J. (Ed.), 1999. Investigational program of hydrogeology and hydrochemistry. In: Short-term programme of qualifying the Boda Claystone Formation. Final Report of Research, (in Hungarian) Mecserkérc Co., Pécs, vol. 5, p. 117.

Davy, C.A., Skoczylas, F., Barnichon, J.-D., Lebon, P., 2007. Permeability of macro-cracked argillite under confinement: gas and water testing. Physics and Chemistry of the Earth vol. 32, 667–680.

Dicker, A.I., Smits, R.M., 1988. A practical approach for determining permeability from laboratory pressure-pulse decay measurements. SPE, 17578.

Jones, S.C., 1997. A technique for faster pulse-decay permeability measurements in tight rocks. SPE Formation Evaluation, 19–25. March.

Kovács, L. (Ed.), 1999. Digest on the results of the short-term characterisation programme of the Boda Claystone Formation. Pécs-Paks, 62.

Lakatos, I., Fedor F., Tóth, J., 2002. Hydrodynamical examinations of cores originated from Boda Claystone Formation, Hungary, Report (in Hungarian).

Lee, A.L., Gonzalez, M.H., Eakin, B.E., 1966. The viscosity of natural gases. Journal of Petroleum Technology, 997–1000. August.

Lowell, S., Shields, J.E., 1991. Powder Surface Area and Porosity. Chapman and Hall, London. pp. 99–120.

Máthé, Z. (Ed.), 1998. Minerological, petrological, rock geochemical and isotope transport analysis. In: Short-term programme of qualifying the Boda Claystone Formation, Final Report of Research, (in Hungarian) Mecserkérc Co., Pécs, vol. 4, p. 76.

McLennan, S.M., 2001. Relationships between the trace element composition of sedimentary rocks and upper continental crust. Geochemistry, Geophysics, Geosystems 2, 24 (2000GC000109).

Meehan, D.N., 1980. A correlation for water compressibility. Petroleum Engineer 56, 125–126. November.

Report, Pécs, Mecsek Ércbányászati Vállalat (MÉV), 1993. Report on the results of geological research of the proposed Mecsek deep repository between 1989–1992. (manuscript) Taylor, S.R., McLennan, S.M., 1985. The Continental Crust: its Composition and Evolution. Blackwell, Oxford, 312p.

Numbere, D., Brigham, W.E., Standing, M.B., 1977. Correlations for Physical Properties of Petroleum Reservoir Brines, vol. 1977. Petroleum Research Institute, Stanford University. November, p. 8.

SzKFI Report, 1990. Measurement of permeability under constant overburden pressure, and porosity of lower Permian aleurolite samples on varying pore pressure and temperature, (in Hungarian), Nagykanizsa, (manuscript).

SzKFI Report, 1991. Measurement of permeability under constant overburden pressure, and porosity of lower Permian aleurolite samples on varying pore pressure and temperature, (in Hungarian), Nagykanizsa, (manuscript).

Varga, R.A., Szakmány, Gy., Raucsik, B., Máthé, Z., 2005. Chemical composition, provenance and early diagenetic processes of playa lake deposits from the Boda Siltstone Formation (Upper Permian), SW Hungary. Acta Geologica Hungarica vol. 48, 49–68.

Varga, A., Raucsik, B., Szakmány, Gy., Máthé, Z., 2006. Minerological, petrological and geochemical character of clastic rock types of BCF (in Hungarian). Földtani Közlöny vol. 136/2, 201–232.